Supporting Information

Flexible Superhydrophobic Metal-based Carbon Nanotube Membrane for Electrochemically Enhanced Water Treatment

Yiran Si[a], Chunyi Sun[a], Dongfeng Li[b], Fenglin Yang[a], Chuyang Y. Tang[c], Xie Quan[a], Yingchao Dong[a], Michael D. Guiver[d*]*

[a] Key Laboratory of Industrial Ecology and Environmental Engineering (Ministry of Education, MOE), School of Environmental Science and Technology, Dalian University of Technology, Dalian 116024, China

[b] School of Science, Harbin Institute of Technology, Shenzhen 518055, China

[c] Department of Civil Engineering, The University of Hong Kong, Pokfulam, Hong Kong S.A.R., China

[d] State Key Laboratory of Engines, and Collaborative Innovation Center of Chemical Science and Engineering (Tianjin), Tianjin University, Tianjin 300072, China

Note: Yiran Si and Chunyi Sun made equal contributions to this work.

Corresponding authors:

Prof. Michael D. Guiver

State Key Laboratory of Engines, and Collaborative Innovation Center of Chemical Science and Engineering (Tianjin), Tianjin University, Tianjin 300072, China

Tel: +86-158-22869113 E-mail: guiver@tju.edu.cn

Prof. Yingchao Dong

Key Laboratory of Industrial Ecology and Environmental Engineering (Ministry of Education, MOE), School of Environmental Science and Technology, Dalian University of Technology, Dalian 116024, China

Tel: +86-411-84706328 E-mail: ycdong@dlut.edu.cn

Number of pages (including the cover page): 17

Number of figures: 6

Number of tables: 4

Page S3, S1. Illustration of the preparation and VMD process of SS-CNT membrane

Page S4, S2. Preparation and characterization of SSHF membrane substrate

Page S8, S3. Properties and cost of SS-CNT membrane

Page S10, S4. TEM and HRTEM images of CNTs

Page S11, S5. EDS element mapping analysis of oxidized SS-CNT membrane surfaces

Page S12, S6. Evaluation of energy consumption

Page S14, S7. Performance comparison with other membranes

S1 Illustration of the preparation and VMD process of SS-CNT membrane

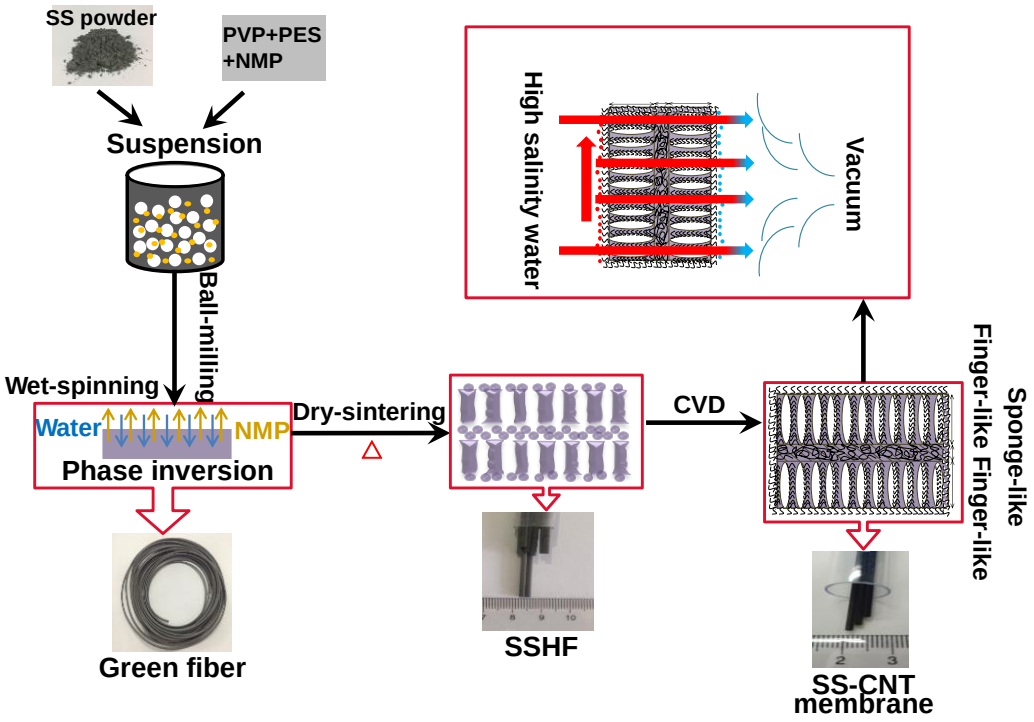

Figure S1. Illustration of the preparation and vacuum membrane distillation (VMD) process of SS-CNT membrane with details about the key steps, sample images and simplified structure models.

Stainless steel hollow fiber (SSHF) membrane substrate with an asymmetric sandwich structure was prepared by a sequential process of immersion-induced phase inversion and dry-sintering. By employing a simple and cost-effective surface activation followed by self-catalyzed chemical vapor deposition (CVD), CNT was functionally constructed *in situ* on SS substrates to form superhydrophobic SS-CNT membrane. Subsequently, vacuum membrane distillation (VMD) performance of SS-CNT membrane for the treatment of high salinity water was systematically investigated.

S2 Preparation and characterization of SSHF membrane substrate

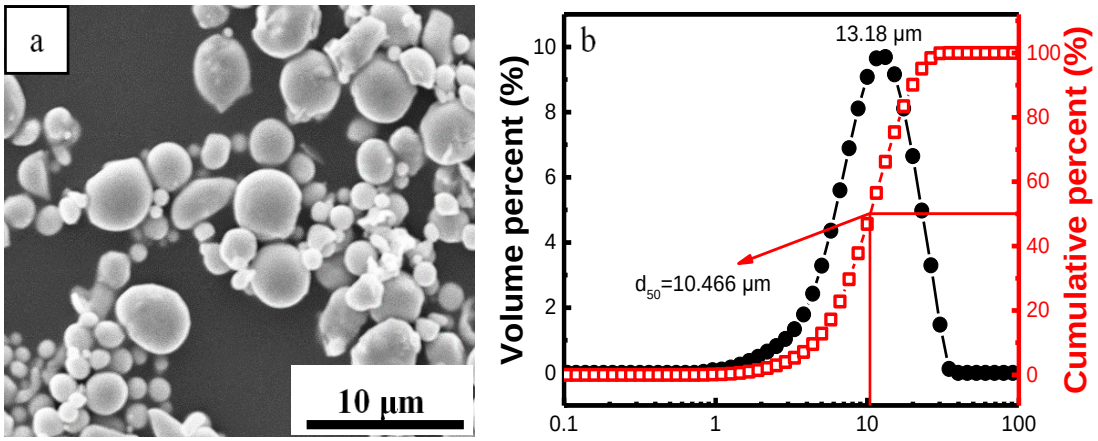

Figure S2. (a) SEM image, (b) particle size distribution of 316L stainless steel powder.

The 316L stainless steel particles exhibit smooth surfaces with spheroidal shapes (Figure S2a). The particle size was measured by a laser particle size analyzer (Marvin 2000, Malvern instruments Ltd., UK). The 316L SS powder has a particle size of D_{50} = 10.5 μm (Figure S2b).

S2.1 Preparation procedures of SSHF membrane substrate

Table S1. Suspension compositions and dry-wet spinning parameters of SS hollow fiber membrane substrates.

Spinning parameters	Conditions
Solids loading (wt.%)	75
PES + NMP (wt.%)	25 (PES: NMP = 1:4)
PVP (g)	3
Temperature (°C)	25
Internal/ External coagulant	Deionized water/ Tap water
Bore liquid flow rate ($mL \cdot min^{-1}$)	50
Nitrogen pressure (MPa)	0.05
Air gap (cm)	10

Generally, PES and PVP were dissolved in NMP under constant stirring of 30 rpm for 6 h to form a homogeneous polymer solution. The mass ratio of PES to NMP was 1:4. SS powder (75 wt.%) was gradually added to the above solution, while stirring was maintained for 60 h, to form a uniform suspension. The suspension was vacuum-degassed for about 1 h at room temperature to remove air bubbles. After degasification, the suspension was poured into a reservoir leading to a laboratory-made tube-in-orifice spinneret (inner and outer diameters of 1.3 mm and 2.5 mm, respectively) under a nitrogen pressure of 0.05 MPa. Tap water and deionized water were used as the external and internal coagulants, respectively. Deionized water was pumped through the bore of the spinneret at a flow rate of 50 $mL \cdot min^{-1}$. The air gap between the spinneret and the coagulant bath was adjusted to 10 cm. The green-body hollow fibers were immersed in tap water for 24 h to ensure a sufficient exchange between NMP solvent and non-solvent water, and then dried in air at room temperature (25 °C). Details of the preparation parameters are presented in Table S1.

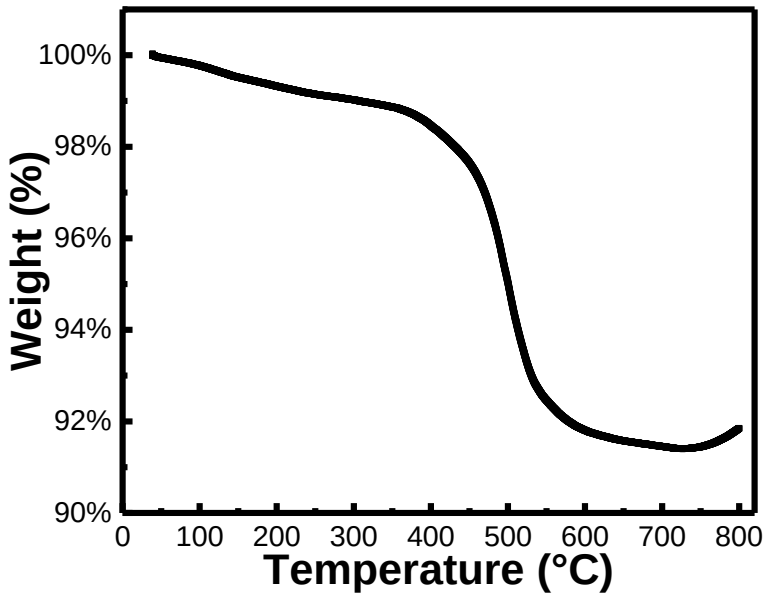

Figure S3. TGA curve of the dried SSHF membrane substrate green body heated between 40 °C and 800 °C under hydrogen atmosphere.

The precursor hollow fibers were sintered in a tube furnace (OTF-1200X-S, Hefei Kejing Material Technology Co., Ltd., China), at 200 °C for 0.5 h and then 600 °C for 0.5 h respectively in H_2 with a flow rate of 60 mL·min^{-1} to remove residual water and the organic polymers (based on the TGA analysis in Figure S3). They were then sintered at 1050 °C for 1 h. Finally, hydrogen (H_2) was used to cool the reactor to room temperature (25 °C).

In order to compare the electronic conductivity of the SSHF membrane substrate prepared in this work with alumina (Al_2O_3) ceramic membrane substrate (see Section "Mechanical and Electrical properties of Substrates"), Al_2O_3 ceramic membrane substrate was prepared by a dry-wet-spinning technique involving immersion-induced phase inversion process. The prepared fiber membrane precursors were then sintered at 1250 °C in air to obtain the final hollow fiber Al_2O_3 ceramic substrates. Electrochemical

impedance spectroscopy (EIS) of Al_2O_3 ceramic membrane substrate was performed using an electrochemical workstation.

S2.2 Characterization of SSHF membrane substrate

The mechanical strength of SSHF membrane substrates was measured by the three-point bending test using a universal testing machine (AGS-X, Shimadzu (Suzhou) Instruments Manufacturing Co., Ltd., China). During the test, the substrate was placed on a span of 8 mm and then loaded at a crosshead speed of 0.02 $mm \cdot min^{-1}$ until fracture occurred. Twenty samples for each set were tested to obtain an average value. The bending strength (σ_F, MPa) was calculated using equation S1:[1,2]

$$\sigma_F = \frac{8FLD}{\pi(D^4 - d^4)} \quad \text{(S1)}$$

where F is the measured force (N) at which fracture takes place, and L is the span (mm). D and d are the outer and inner diameters (mm) of SSHF membrane substrate, respectively.

Nitrogen permeance of SSHF membrane substrate was measured by a Micro-Filtration Membrane Porometer (PSDA-20, Nanjing GaoQ Functional Materials Co., Ltd., China). Each sample measurement was repeated three times. The gas permeance (P, $mol \cdot m^{-2} \cdot Pa^{-1} \cdot s^{-1}$) was calculated using equation S2:

$$p = \frac{Q \ln(D/d)}{\pi L (D-d) \Delta P}$$

where Q, D, d, L and ΔP are the nitrogen permeation rate ($mol \cdot s^{-1}$), the outer diameter (m) and the inner diameter (m) of SSHF membrane substrate, the hollow fiber length

(m), and the trans-membrane pressure difference (Pa), respectively.

The pure water flux of the SSHF membrane substrate was measured by a laboratory-made crossflow filtration apparatus.[3] Before the tests, all the substrates were ultrasonically cleaned with ethanol for 10 min. Pure water was filtered through SSHF membrane substrates at an operating pressure of 0.1 bar. Each sample measurement was repeated three times.

S3 Properties and cost of SS-CNT membrane

S3.1 Pore size and flux

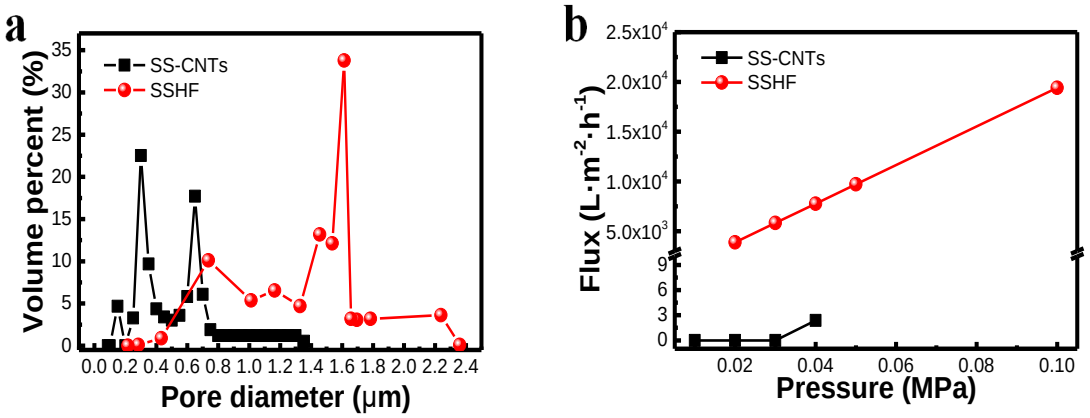

Figure S4. (a) Pore size distribution and (b) pure water flux under different trans-membrane pressures of SSHF membrane and SS-CNT membrane.

As shown in Figure S4a, the average pore size of the SSHF membrane was 1.60 μm after sintering at 1050 °C, while the SS-CNT membrane has a relatively smaller pore size of 0.57 μm. In addition, the pure water permeability of SSHF membrane was measured to be 19408 $L \cdot m^{-2} \cdot h^{-1} \cdot bar^{-1}$, whereas liquid water permeation was not detected for SS-CNT membrane until a N_2 pressure of 0.4 bar, indicating a liquid entry pressure of 0.4 bar (Figure S4b).

S3.2 Cost of SS-CNT membrane

Table S2. The cost of SS-CNT membrane fabricated in this work.

	Material cost (¥·m^{-2})	Sintering cost (¥·m^{-2})		Total cost (¥·m^{-2})
		Atmosphere	Electricity	
SS-CNT membrane	62	22	147	231

For the SS-CNT membrane, the total cost per unit membrane area is mainly material cost (stainless steel power and various additives), sintering cost for the SS substrate (electricity energy and H_2 gas consumption) and for SS-CNT membrane (electrical energy and C_2H_4/H_2 gas consumption). The total calculated materials and consumables costs of the SS-CNT membrane in this work is estimated to be 231 ¥·m^{-2} (Table S2). In China, the current purchase price of commercial polymer membranes such as polytetrafluoroethylene (PTFE), polypropylene (PP) and poly(vinylidene fluoride) (PVDF) are approximately in the range of 200~500 ¥·m^{-2}. The reasonable materials and consumables costs of fabricating SS-CNT membranes suggest a good potential in practical MD applications. However, different from market price, this calculation is based solely on the materials and consumables costs of lab-scale fabrication, and does not include other typical business cost elements such as manpower, marketing, distribution and profits.

S4 TEM and HRTEM images of CNTs

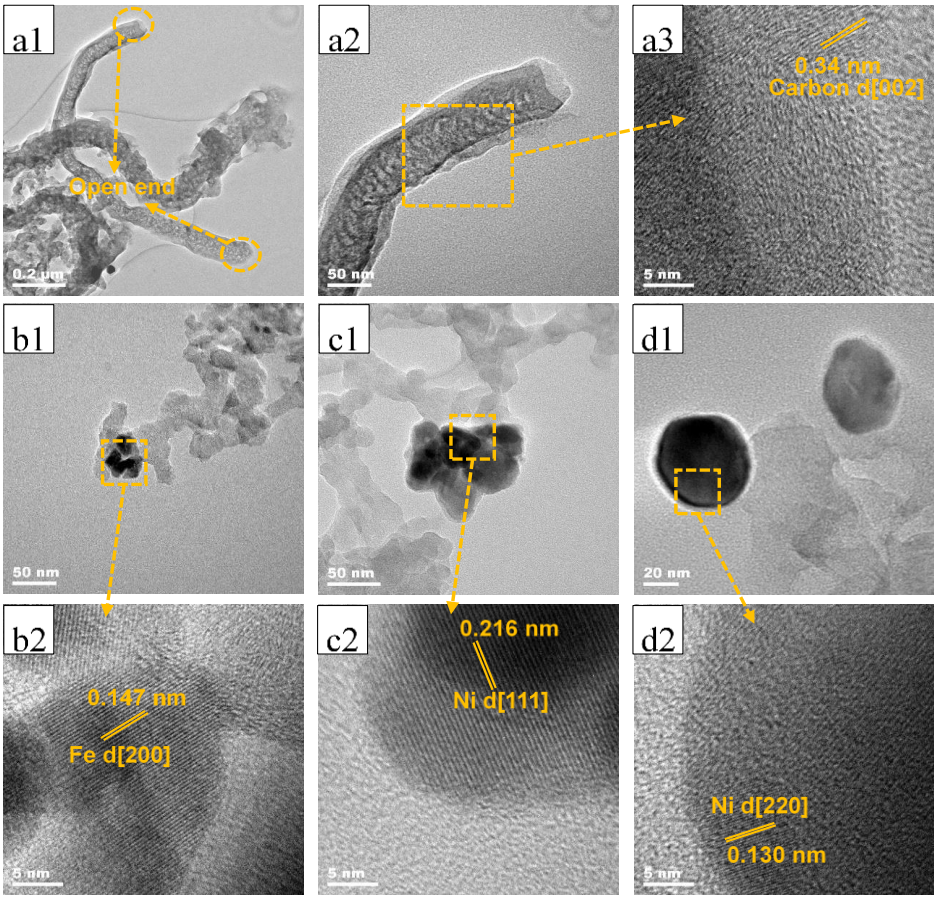

Figure S5. (a1-a2) TEM and (a3) HRTEM images of CNTs; TEM images of CNTs with Fe particles (b1) or Ni particles (c1-d1) on the tip and HRTEM images of Fe particles (b2) or Ni particles (c2-d2) inside the formed CNTs.

Figure S5 shows the TEM and HRTEM images of CNTs observed in our samples. The TEM results confirm that CNTs have a hollow structure with an open end (Figures S5a1-a2). The distance between two adjacent crystalline planes, d-spacing, was determined to be 0.34 nm (Figure S5a3), which corresponds to the characteristic (002) reflection of CNTs.[4] Two different types of catalyst particles are observed at the tip of CNTs in Figures S5b1-d1, which correlate with the lattice fringes of Fe and Ni catalysts derived from the *in situ* reduction of Fe_2O_3 and NiO inherent in the SS substrates

(Figures S5b2-d2). This observation also confirms that a tip-growth model mechanism was dominant.

S5 EDS element mapping analysis of oxidized SS-CNT membrane surfaces

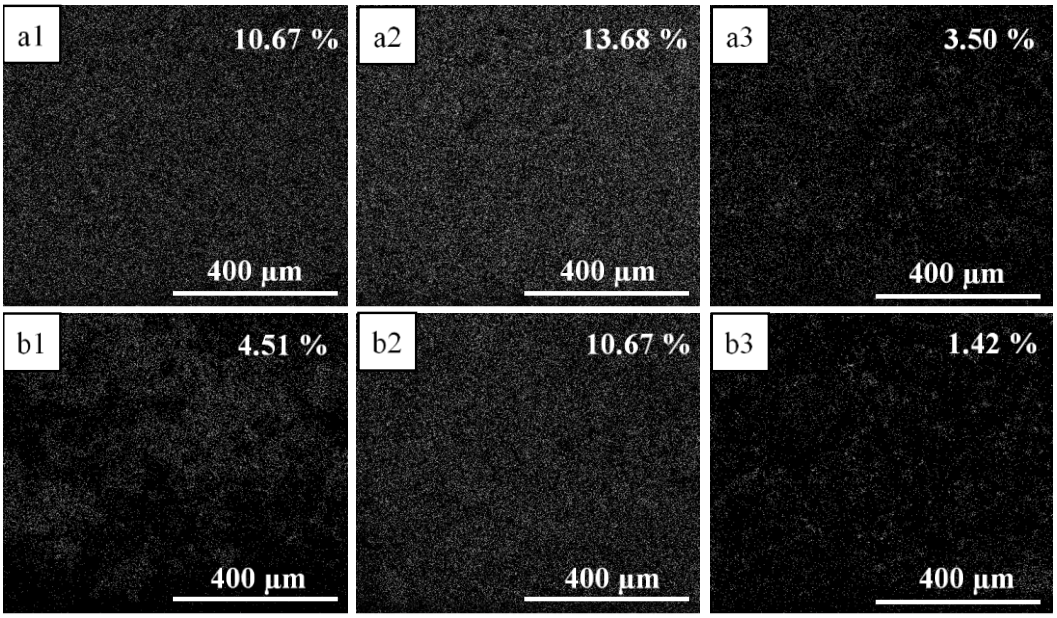

Figure S6. EDS element (Fe) mapping analysis of the oxidized surface of SS-CNT membrane for the treatment of the feeds with different salinities ((a) 35 g·L^{-1} NaCl, (b) 70 g·L^{-1} NaCl) after 6 h VMD operation at different electro-chemical conditions: (1) 0 V open circuit, (2) +2.0 V positive polarization, (3) -2.0 V negative polarization. The value% in each graph represents the elemental percentage for Fe.

Figure S6 shows EDS element (Fe) mapping analysis of the oxidized surface of SS-CNT membrane for treatment of the feeds with different salinities under different voltages after 6 h operation. For these two feeds (35 g·L^{-1} and 70 g·L^{-1} NaCl), compared with open circuit (Figures S6a1 and S6b1), a stronger Fe signal (higher content) was observed under positive polarization (+2.0 V) (Figures S6a2 and S6b2), indicating significant corrosion behavior. A much weaker Fe signal (much lower content) was observed under negative polarization, due to the significantly enhanced anti-corrosion

function via a cathodic protection mechanism (Figures S6a3 and S6b3). Therefore, a negative polarization micro-electric field-coupling strategy enhances the anti-corrosion performance of SS-CNT membranes.

Table S3. The elemental percentage for Fe and O of the SS-CNT membrane for treatment of an organic high salinity feed (70 $g \cdot L^{-1}$, NaCl, 30 $mg \cdot L^{-1}$, HA) after 6 h VMD operation under different voltages.

	Condition	Element	
		O	Fe
Atomic percentage (%)	0 V	20.5	5.92
	+2 V	56.21	11.48
	-2 V	8.57	1.63

Table S3 shows the elemental percentage for Fe and O of the SS-CNT membrane for treatment of the organic high salinity feed (70 $g \cdot L^{-1}$, NaCl, 30 $mg \cdot L^{-1}$, HA) after 6 h VMD operation under different voltages. Compared with those (Fe, 5.92% and O, 20.5%) under open circuit, a higher elemental percentage of Fe (11.48%) and O (56.21%) was detected under positive polarization, indicating significant corrosion behavior. However, a much lower elemental percentage of Fe (1.63%) and O (8.57%) was obtained under negative polarization, due to significantly enhanced anti-corrosion function via a micro-electric field coupling strategy.

S6 Evaluation of energy consumption

During the VMD process, the energy consumption for SS-CNT membranes with and

without applying electricity can be calculated based on the following equation (S3):

$$W = \frac{(W_0 + W_e)}{J_0 / J_1}$$

Where W (kW·h·m^{-3}) is the total energy consumed per unit volume water production with electric field, W_0 (kW·h·m^{-3}) is the energy consumed per unit volume water production without electric field, W_e (kW·h·m^{-3}) is the electricity energy consumed per unit volume water production with electric field, J_0 (L·m^{-2}·h^{-1}) is the permeate flux with electric field, and J_1 (L·m^{-2}·h^{-1}) is the permeate flux without electric field.

Moreover, W_e can be calculated according to the following equation (S4):[5]

$$W_e = \frac{U \cdot (\frac{I}{A}) \times 10^{-3}}{J \times 10^{-3}} \cdot 1h \qquad \text{(S4)}$$

Where W_e (kW·h·m^{-3}) is the electricity energy consumed per unit volume water production with electric field, U (V) is direct current potential (2 V, in this work), I (A) is the current, A (m^2) is the effective membrane area, J (L·m^{-2}·h^{-1}) is the permeate flux.

In this work, W_0 is calculated to be 46.69 kW·h·m^{-3}, which is higher that of W (37.78 kW·h·m^{-3}), showing that ~8.91 kW·h·m^{-3} can be saved during the VMD process using electric field. Significantly improved water flux was observed at -2.0 V for 6 h, much higher (~1.25 times) than that under open circuit, while energy consumption could be also reduced to 37.78 kW·h·m^{-3}. Compared with conventional VMD without applying electric field, these results suggest that electrochemically-assisted VMD can save about 19.08% energy, which is also 3.3 times higher than the 5.74% energy consumption

saving for spinel-CNTs membrane at the same operation conditions.[5]

S7 Performance comparison with other membranes

Table S4 shows performance comparison between existing state-of-the-art polymeric membranes and SS-CNT membrane (this work) for MD application. SS-CNT membrane exhibits a much higher water contact angle (~171°), outperforming all the polymeric membranes such as poly(vinylidene fluoride) (PVDF), polytetrafluoroethylene (PTFE) and poly(tetrafluoroethylene-*co*-hexafluoropropylene) (FEP). Such an excellent superhydrophobicity characteristic is beneficial for MD, through efficiently inhibiting water penetration and pore wetting while enabling rapid vapor transport across the membrane pores.[6] Interestingly, the permeate flux of SS-CNT membrane exhibits a high level of 29.0 $L \cdot m^{-2} \cdot h^{-1}$ for simulated seawater (35 $g \cdot L^{-1}$ NaCl), outperforming many existing polymeric membranes, with the exception of PVDF.[7,8] Nevertheless, it is reasonable to expect that permeate flux can be further enhanced for the SS-CNT membrane after optimizing membrane structure, module design, and operating parameters such as feed temperature and vacuum level.

Table S4. Comparison of properties and MD performances between SS-CNT membrane in this work and those reported in the literature.

		Membrane				Operation parameter		Performance		
MD	Material	Configuration	Pore size (nm)	Contact angle (°)	LEP (bar)	Solution	ΔT (°C)	Permeation flux ($L \cdot m^{-2} \cdot h^{-1}$)	Rejection (%)	Refs.
DCMD*	PVDF*	hollow fiber	500	105	NA*	35 $g \cdot L^{-1}$ NaCl	62	40.5	99.99	[7]
DCMD	PVDF	flat sheet	490	145	NA	35 $g \cdot L^{-1}$ NaCl	48	18.9	99.8	[9]
DCMD	PVDF	hollow fiber	186	103	NA	35 $g \cdot L^{-1}$ NaCl	62	46.1	99.8	[8]
DCMD	PVDF	flat sheet	210	136	0.35	35 $g \cdot L^{-1}$ NaCl	30	20.6	NA	[10]
VMD*	PTFE*	hollow fiber	120	127	3.5	30 $g \cdot L^{-1}$ NaCl	65	17.2	99.9	[11]
VMD	FEP*	hollow fiber	NA	117	2.4	35 $g \cdot L^{-1}$ NaCl	75	8.4	>99.7	[12]
VMD	PVDF	hollow fiber	NA	139	7.0	35 $g \cdot L^{-1}$ NaCl	70	10.0	>99.9	[13]
VMD	PVDF	hollow fiber	107	145	4.5	35 $g \cdot L^{-1}$ NaCl	70	7.9	>99.9	[14]
VMD	PVDF	hollow fiber	165	NA	3.0	35 $g \cdot L^{-1}$ NaCl	60	26.5	NA	[15]
VMD	PVDF	flat sheet	340	151	3.8	Imitated sea water	60	28.1	99.9	[16]
VMD	PP*	flat sheet	200	NA	NA	100 $g \cdot L^{-1}$ NaCl	55	14.4	NA	[17]
VMD	SS-CNT	hollow fiber	569	171	0.4	35 $g \cdot L^{-1}$ NaCl	75	29.0	>99.9	This work

*Notes: DCMD: direct contact membrane distillation, VMD: vacuum membrane distillation, PVDF: poly(vinylidene fluoride), PTFE: polytetrafluoroethylene, PP: polypropylene, FEP: poly(tetrafluoroethylene-*co*-hexafluoropropylene), LEP: liquid entry pressure, NA: not available.

References

(1) Schmeda-Lopez, D. R.; Smart, S.; Nunes, E. H.; Vasconcelos, D.; Vasconcelos, W. L.; Bram, M.; Meulenberg, W. A.; da Costa, J. C. D. Stainless steel hollow fibres–Sintering, morphology and mechanical properties. *Sep. Purif. Technol.* **2015,** *147*, 379-387.

(2) Michielsen, B.; Chen, H.; Jacobs, M.; Middelkoop, V.; Mullens, S.; Thijs, I.; Buekenhoudt, A.; Snijkers, F. Preparation of porous stainless steel hollow fibers by robotic fiber deposition. *J. Membr. Sci.* **2013,** *437*, 17-24.

(3) Chen, M.; Zhu, L.; Chen, J.; Yang, F.; Tang, C. Y.; Guiver, M. D.; Dong, Y. Spinel-based ceramic membranes coupling solid sludge recycling with oily wastewater treatment. *Water Res.* **2020,** *169*, 115180.

(4) Zhu, L.; Dong, X.; Xu, M.; Yang, F.; Guiver, M. D.; Dong, Y. Fabrication of mullite ceramic-supported carbon nanotube composite membranes with enhanced performance in direct separation of high-temperature emulsified oil droplets. *J. Membr. Sci.* **2019,** *582*, 140-150.

(5) Dong, Y.; Ma, L.; Tang, C. Y.; Yang, F.; Quan, X.; Jassby, D.; Zaworotko, M. J.; Guiver, M. D. Stable superhydrophobic ceramic-based carbon nanotube composite desalination membranes. *Nano Lett.* **2018,** *18* (9), 5514-5521.

(6) Deshmukh, A.; Boo, C.; Karanikola, V.; Lin, S.; Straub, A. P.; Tong, T.; Warsinger, D. M.; Elimelech, M. Membrane distillation at the water-energy nexus: limits, opportunities, and challenges. *Energy Environ. Sci.* **2018,** *11* (5), 1177-1196.

(7) Hou, D.; Wang, J.; Qu, D.; Luan, Z.; Ren, X. Fabrication and characterization of hydrophobic PVDF hollow fiber membranes for desalination through direct contact membrane distillation. *Sep. Purif. Technol.* **2009,** *69* (1), 78-86.

(8) Teoh, M. M.; Chung, T. Membrane distillation with hydrophobic macrovoid-free PVDF-PTFE hollow fiber membranes. *Sep. Purif. Technol.* **2009,** *66* (2), 229-236.

(9) Fan, H.; Peng, Y. Application of PVDF membranes in desalination and comparison of the VMD and DCMD processes. *Chem. Eng. Sci.* **2012,** *79*, 94-102.

(10) Liao, Y.; Wang, R.; Tian, M.; Qiu, C.; Fane, A. G. Fabrication of polyvinylidene fluoride (PVDF) nanofiber membranes by electro-spinning for direct contact membrane distillation. *J. Membr. Sci.* **2013,** *425*, 30-39.

(11) Zhu, H.; Wang, H.; Wang, F.; Guo, Y.; Zhang, H.; Chen, J. Preparation and properties of PTFE hollow fiber membranes for desalination through vacuum membrane distillation. *J. Membr. Sci.* **2013,** *446*, 145-153.

(12) Chen, K.; Xiao, C.; Huang, Q.; Liu, H.; Liu, H.; Wu, Y.; Liu, Z. Study on vacuum membrane distillation (VMD) using FEP hollow fiber membrane. *Desalination* **2015,** *375*, 24-32.

(13) Tong, D.; Wang, X.; Ali, M.; Lan, C. Q.; Wang, Y.; Drioli, E.; Wang, Z.; Cui, Z. Preparation of Hyflon AD60/PVDF composite hollow fiber membranes for vacuum membrane distillation. *Sep. Purif. Technol.* **2016,** *157*, 1-8.

(14) Zhang, Y.; Wang, X.; Cui, Z.; Drioli, E.; Wang, Z.; Zhao, S. Enhancing wetting resistance of poly(vinylidene fluoride) membranes for vacuum membrane distillation. *Desalination* **2017,** *415*, 58-66.

(15) Zuo, J.; Chung, T. PVDF hollow fibers with novel sandwich structure and superior wetting resistance for vacuum membrane distillation. *Desalination* **2017,** *417*, 94-101.

(16) Sun, Q.; Yang, Z.; Hu. C.; Li, C.; Yan, G.; Wang, Z. Facile preparation of superhydrophobic PVDF microporous membranes with excellent anti-fouling ability for vacuum membrane distillation. *J. Membr. Sci.* **2020,** *605*, 118106.

(17) Safavi, M.; Mohammadi, T. High-salinity water desalination using VMD. *Chem. Eng. J.* **2009,** *149* (1), 191-195.